ISTS 2006-k-09

TERRAMECHANICS-BASED ANALYSIS ON SLOPE TRAVERSABILITY FOR A PLANETARY EXPLORATION ROVER

Genya Ishigami, Akiko Miwa, Keiji Nagatani, Kazuya Yoshida
Department of Aerospace Engineering, Tohoku University
Aoba 6-6-01, Sendai, 980-8579, JAPAN
(E-mail : ishigami@astro.mech.tohoku.ac.jp)

Abstract

This paper describes slope traversability analysis for a planetary exploration rover based on a terramechanics approach. In this research, the slope traversability is defined as consisting both of slope climbing and traversing (crossing) capabilities. The authors have been investigated traction mechanics between a wheel of a rover and loose soil. Applying our advantages in the wheel-soil interactions to the slope traversability of a rover, two criteria dominating the slope traversability, named as "Mobility limit" and "Trafficability limit," are investigated. The mobility limit is determined by a margin between the torque limit of a wheel driving motor and the resistance torque to the wheel. The trafficability limit is also determined by a relationship between the traction load of a rover and the summation of traction forces generated by wheels. Through a number of slope climbing/traversing experiments using our rover test bed, the slope traversability of the rover is evaluated by the proposed criteria.

1. Introduction

An investigation of inner constituents of a planetary body is an important mission to bring out the origin of the planetary body. It is known that an exploration into a crater of a planetary body is one of the effective approaches to investigate inner constituents of the planet, because a central peak in the crater (relatively large scale one) can consist of materials that protuberated by a meteorite impact from some ten kilometers depth of the planetary body.

A planetary rover is one of the key technologies to explore into the crater. The rover has to have enough capabilities to travel highly challenging terrain, climb or traverse slopes of the crater. However, the planetary surface terrain including craters, such as on the Moon or the Mars, is mostly covered with fine-grain loose soil called regolith. Negotiating with slopes around the crater is then difficult task since wheels of the rover might easily slip or loose their tractions on such loose soil. In addition, those slips will increase when the rover climbs or traverses the slope. It is deduced that slopes climbing/traversing capabilities, in other words, the slope traversability of the rover will be dominated by a dynamic interaction between wheels and loose soil.

The research field regarding the wheel-soil interaction has been investigated in a filed called "Terramechanics." For instance, an analysis of a wheel-soil interaction mechanism and a modelling of stress distributions underneath a wheel have been well studied in [1]-[3]. Iagnemma et al. have applied those terramechanics models to traction mechanics of planetary rovers [4][5]. We have elaborated a wheel-and-vehicle dynamics model, which is able to deal with motion characteristics for planetary rovers [6]-[7]. A slope climbing capability of a rover has been also discussed in a paper [6], however, detailed criteria to determine the slope traversability of a rover are still left as an open issue.

In this paper, the slope traversability analysis based on the terramechanics approach is addressed with applying our background in regard to the dynamic interaction of a wheel on loose soil. The wheel-soil contact model developed in our previous works has to be improved to deal with a wheel on an inclined surface. Also, to clarify characteristics of wheel forces/torque (a drawbar pull, a side force and a resistance torque), we have carried out single wheel experiments and numerical simulations.

Then, the slope traversability criteria are proposed through discussing the characteristics of the wheel forces and torque. One of the criteria is named "Mobility limit," and the other is "Trafficability limit." The mobility limit is simply caused by a relationship between a torque limit of a wheel driving motor and a resistance torque to the wheel. On the other hand, the trafficability limit is determined by a traction load of a rover and a summation of wheels' forces (drawbar pulls and side forces.)

Additionally, the slope climbing/traversing experiments using our rover test bed are carried out in order to analyze the slope traversability of the rover. According to those slope experiments, it is found that the proposed criteria are able to evaluate the slope traversability of the rover.

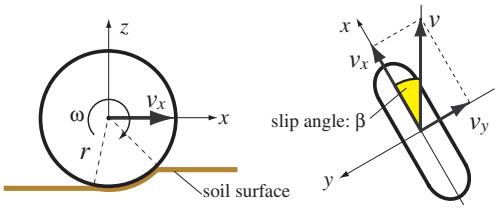

Fig. 1: Wheel coordinate system

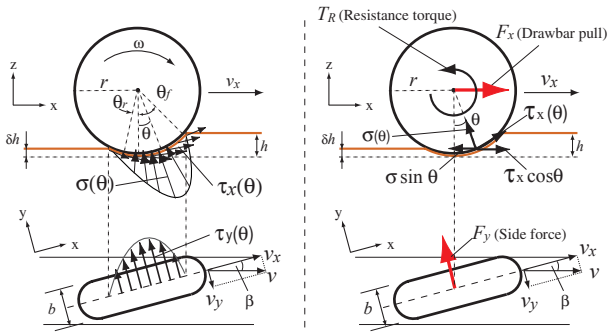

(a) : Stress model (b) : Force model

Fig. 2: Wheel-soil contact model

2. Wheel-Soil Contact Model

The following analysis deals with a rigid wheel which rotates on loose soil. A wheel coordinate system is defined using a right-hand frame as shown in Fig. 1, where the longitudinal direction is denoted by x, the lateral direction by y, and the vertical direction by z. The coordinate frame turns according to a steering action of the wheel (the yaw rotation around the z axis) but does not rotate with a driving motion of the wheel (the pitch rotation around the y axis).

2.1 Slip ratio and slip angle

When a wheel travels on loose soil, the wheel slips both in the longitudinal and lateral directions, respectively. The slip in the longitudinal direction is measured by "slip ratio," which is defined as a function of the longitudinal traveling velocity v_x and the circumference velocity of the wheel $r\omega$:

$$s = \begin{cases} (r\omega - v_x)/r\omega & (r\omega > v_x : \text{driving}) \\ (r\omega - v_x)/v_x & (r\omega < v_x : \text{braking}) \end{cases} \quad (1)$$

The slip ratio takes a value between -1 and 1.

On the other hand, the slip in the lateral direction is measured by "slip angle," which is defined by the longitudinal and lateral traveling velocities v_y of the wheel as follows:

$$\beta = \tan^{-1}(v_y/v_x) \quad (2)$$

2.2 Normal stress and shear stress

To deal with a normal stress and a shear stress of a wheel is quite needed to obtain wheel forces. Based on terramechanics models, the stresses under the wheel can be modeled as shown in Fig. 2-(a).

The normal stress $\sigma(\theta)$ is described according to [7]:

$$\sigma(\theta) = \begin{cases} \sigma_m \left(\frac{\cos\theta - \cos\theta_f}{\cos\theta_m - \cos\theta_f} \right)^n & (\theta_m \le \theta < \theta_f) \\ \sigma_m \left(\frac{\cos\{\theta_f - \frac{\theta - \theta_r}{\theta_m - \theta_r}(\theta_f - \theta_m)\} - \cos\theta_f}{\cos\theta_m - \cos\theta_f} \right)^n & (\theta_r < \theta \le \theta_m) \end{cases} \quad (3)$$

θ_m is the specific wheel angle at which the normal stress is maximized:

$$\theta_m = (a_0 + a_1 s)\theta_f \quad (4)$$

where a_0 and a_1 are soil parameters. The values of them are generally assumed as $a_0 \approx 0.4$ and $0 \le a_1 \le 0.3$ [8]. The maximum stress σ_m is defined by the following equation [3]:

$$\sigma_m = r^n (k_c/b + k_\phi)(\cos\theta_m - \cos\theta_f)^n \quad (5)$$

where, k_c, k_ϕ and n are the soil-specific parameters. b is the width of the wheel.

The shear stresses $\tau_x(\theta)$ and $\tau_y(\theta)$ are written by the same expressions:

$$\tau_i(\theta) = (c + \sigma(\theta)\tan\phi)[1 - e^{-j_i(\theta)/k_i}] \quad (i = x, y) \quad (6)$$

The symbols used in the equation (6) are listed as follows:

- c : cohesion stress of a soil
- ϕ : internal friction angle of a soil
- k_i : shear deformation module in each direction

Also, j_x and j_y, which are soil deformations in each direction, can be formulated as a function of the wheel angle θ:

$$j_x(\theta) = r[\theta_f - \theta - (1 - s)(\sin\theta_f - \sin\theta)] \quad (7)$$
$$j_y(\theta) = r(1 - s)(\theta_f - \theta) \cdot \tan\beta \quad (8)$$

2.3 Drawbar pull : F_x

A general force model for a rigid wheel on loose soil is presented in Fig. 2-(b). Using the normal stress $\sigma(\theta)$ and the shear stress in x direction $\tau_x(\theta)$, a drawbar pull F_x that exerts from the soil to the wheel is calculated by the integral from a entry angle θ_f to a exit angle θ_r [2]:

$$F_x = rb \int_{\theta_r}^{\theta_f} \{\tau_x(\theta)\cos\theta - \sigma(\theta)\sin\theta\} d\theta \quad (9)$$

2.4 Side force : F_y

A side force F_y appears at the lateral direction of the wheel when the wheel or the vehicle makes a steering. The current authors have modeled the side force as follows [7]:

$$F_y = \int_{\theta_r}^{\theta_f} \{rb \cdot \tau_y(\theta) + R_b \cdot (r - h(\theta)\cos\theta)\} d\theta \quad (10)$$

R_b is a reaction resistance generated by a bulldozing phenomenon on a side face of the wheel. R_b is given as a function of a wheel sinkage h.

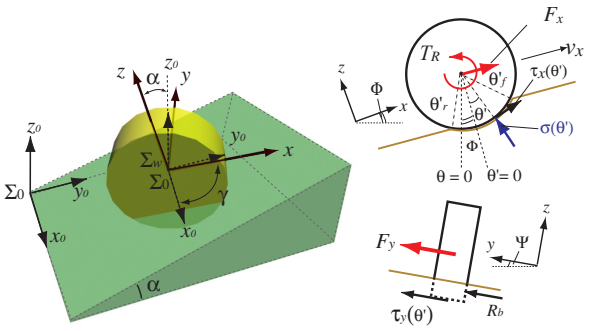

Fig. 3: Definition of the wheel coordinate on inclined surface

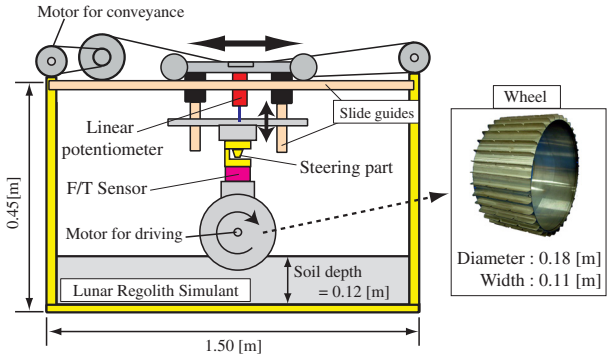

Fig. 4: Schematic view of the single wheel test bed

2.5 Resistance torque : T_R

A resistance torque T_R can be obtained by the integral of the shear stress $\tau_x(\theta)$ as follows [2]:

$$T_R = r^2 b \int_{\theta_r}^{\theta_f} \tau_x(\theta) d\theta \tag{11}$$

2.6 Wheel model on inclined surface

We have applied the wheel-soil contact model to an inclined surface as described in Fig. 3. In the case of the inclined surface, the definition of the wheel coordinate system $\{\Sigma_w\}$ is considered to be equal to the horizontal case. The inclined surface is assumed to be uniform, and a slope angle is denoted by α. When an inertial coordinate system is expressed by $\{\Sigma_0\}$ as a right-hand system, the traverse direction of a slope is denoted by x_0, and the vertical direction by z_0.

The coordinate transformation from $\{\Sigma_0\}$ to $\{\Sigma_w\}$ is employed by a rotation of x_0 axis with α, then another rotation of z_0 axis with γ. The angle composed between a x_0-y_0 planar surface and x (or y) axis is determined by Φ (or Ψ).

As shown in Fig. 3, the wheel angle $\theta^{'}$ is given by $\theta^{'} = \theta - \Phi$, and also $\theta^{'}$ is supposed to be zero in the normal direction of the inclined surface. Note that, stress distributions of a wheel on an inclined surface are assumed to be equivalent to the case of a horizontal surface, not dependent to Φ and Ψ.

Finally, using $\theta^{'}$ instead of θ, wheel forces on an inclined surface can be derived in the same fashion as equations (9), (10) and (11).

3. Single Wheel Experiments and Simulations

Single wheel experiments are carried out to clarify characteristics of both a drawbar pull and a side force. Also the experimental results are compared to numerical simulation results obtained from the wheel-soil contact model.

3.1 Single wheel test bed

Fig. 4 shows the schematic view of the single wheel test bed. The test bed is constituted by both a conveyance unit and a wheel-driving unit. A steering angle (which is equivalent to a slip angle in this test bed) is set between the conveyance unit and the wheel.

Table 1: Simulation parameters and values

parameter	value	unit
c	0.80	[kPa]
ϕ	37.2	[deg]
k_c	1.37×10^3	[N/m^{n+1}]
k_ϕ	8.14×10^5	[N/m^{n+2}]
n	1.00	
k_x	$0.043 \times \beta + 0.036$	[m]
k_y	$0.020 \times \beta + 0.013$	[m]

Encoders that are mounted at both a conveyance motor and a wheel-driving motor respectively measure a translational velocity and an angular velocity of the wheel. Forces and torques generated by the wheel locomotion are measure by a 6-axis force/torque sensor located between a steering part and the wheel. A wheel sinkage is obtained by the use of a linear potentiometer. The wheel with a diameter of 0.18 [m] and a width of 0.11 [m] is covered with paddles of 0.01 [m] heights. The load of the wheel is 64.7 [N].

In the following experiments, the wheel is controlled to rotate with a constant velocity (=0.030 [m/s]) by the driving motor mounted inside of the wheel. The translational velocity of the wheel is also controlled so that a slip ratio of the wheel is set from 0.0 to 0.8 with a step of 0.1. The slip ratio is constant during every single run. Also, the value of a slip angle of the wheel is given from 0 [deg] to 40 [deg] with a step 5 [deg].

A vessel of the single wheel test bed is filled up with 12 [cm] depth of loose soil called “Lunar Regolith Simulant” which is a simulated lunar surface soil regarding similar material components and mechanical characteristics.

3.2 Numerical simulation procedure

The simulations were performed under the same conditions of the single wheel experiments. Parameters used in the simulations are listed in Table 1. The shear deformation modules, k_x and k_y, are given as functions of a slip angle β. A drawbar pull and a side force of a wheel are calculated by equations (9) and (10), respectively. Also, a resistance torque to a wheel is obtained by equation (11).

3.3 Results and discussion

Experimental measurements of a drawbar pull and a side force are respectively plotted in Fig. 5-(a) and

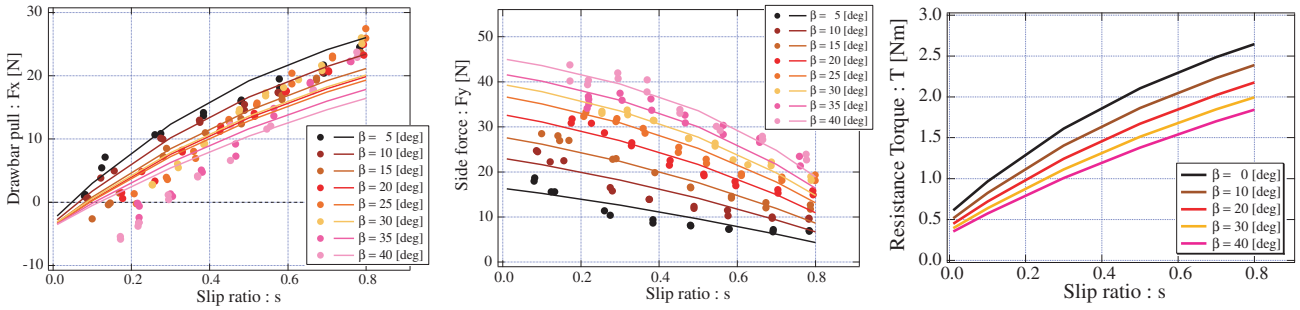

(a) : Slip ratio - Drawbar pull (b) : Slip ratio - Side force (c) : Slip ratio - Resistance torque

Fig. 5: Experimental and simulation results

Fig. 5-(b), for each slip angle from 5 [deg] to 40 [deg]. Theoretical curves calculated by the wheel-soil contact model are also drawn in the corresponding figures.

From Fig. 5-(a), it is seen that the drawbar pull increases as the slip ratio increases, however, decreases depending on the slip angle. Fig. 5-(b) also shows that the side force decreases along with the slip ratio and increases according to the slip angle. The differences between the measured forces and the theoretical values are comparatively small. These results validate that the proposed wheel-soil contact model is able to represent the wheel's traveling behaviors and the contact forces with a reasonable precision.

Regarding the resistance torque, it is relatively difficult to directly measure the torque in the experiments. Therefore, we confirm the characteristics of the resistance torque through the numerical simulation. Theoretical curve of the resistance torque is described in Fig. 5-(c). According to the simulation result, the resistance torque increases with an increase in the slip ratio and decreases as the slip angle increases.

4. Slope Travesability Criteria

The criteria determining the slope traversability of the rover are proposed as "Mobility limit" and "Trafficability limit." These criteria can be explained by the use of the wheel-soil contact model which we developed as mentioned in Section 2.

4.1 Mobility limit

The mobility limit is discussed based on a relationship between a resistance torque and a torque limit of a wheel driving motor. A slip ratio of a wheel on an inclined surface must become larger when a slope angle increases. The resistance torque to a wheel increases along with the slip ratio as already shown in Fig. 5-(c). Then, a wheel driving motor will be suspended if a resistance torque to the wheel is larger than a torque limit of the motor. In a case that one of wheel motors is suspended, resistance torques to the other active wheels must increases and finally all wheel motors will be deactivated. Thus, the mobility limit can be defined as a case when a resistance torque

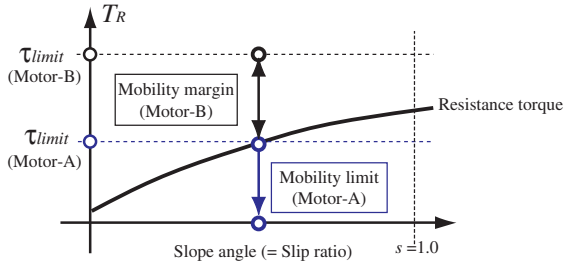

Fig. 6: Mobility limit

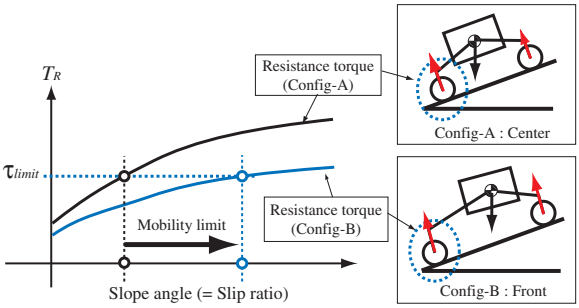

Fig. 7: Improvement of mobility limit

to a wheel T_R equals to or exceeds a torque limit of a wheel motor τ_{limit} as follows:

$$\text{Mobility Limit} \ : \ T_R \geq \tau_{limit}$$

For instance, Fig. 6 describes a theoretical model of the mobility limit. The motor-A in the figure has a small torque limit, therefore, when a resistance torque exceeds its torque limit at an arbitrary slope angle, the mobility limit can be determined at that slope angle. However, if a wheel equips the motor-B having large torque limit instead of the motor-A, the resistance torque never overcome a torque limit of the motor-B even if the slip ratio become 1.0 where the resistance torque is maximized. Then, there is no mobility limit in the case of the motor-B.

In order to improve the mobility limit, the simplest way is to use a high-torque motor. However, it has to be considered that the high-torque motor will expend more energy of a roverfs electric power.

On the other hand, according to the terramechanics theory, a resistance torque of a wheel is originally depended on a vertical load of each wheel if the slip

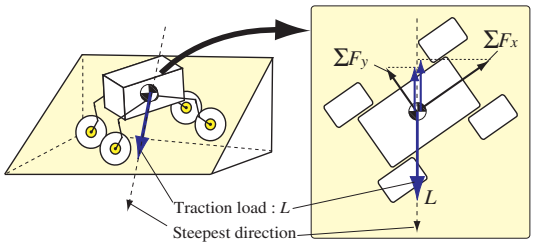

Fig. 8: Trafficability limit

ratio is constant. Thus, equally dividing a vertical load of a rover into each wheel by shifting the centroid of the rover will be also effective to improve the mobility limit. As shown in Fig. 7, it is expected to diminish the resistance torque of the rear wheels of a rover by shifting the centroid of the rover ahead from the Config-A to Config-B.

4.2 Trafficability limit

In order to define the trafficability limit, it is important to consider a balance of forces in the steepest direction at an arbitrary slope as described in Fig. 8. When a traction load L of a rover is larger than a summation of both components of ΣF_x and ΣF_y in the steepest direction, the rover is not able to climb or traverse the slope even if each wheel driving motor has enough torques to avoid the mobility limit. Here, ΣF_x is a summation of drawbar pulls of all wheels, whereas ΣF_y means that of side forces. Thus, the trafficability limit can be obtained when a traction load of a rover L equals to or overcomes a traction force $|\overrightarrow{\Sigma F_x} + \overrightarrow{\Sigma F_y}|$ of the rover as follows:

$$\text{Trafficability Limit} \ : \ L \geq \left|\overrightarrow{\Sigma F_x} + \overrightarrow{\Sigma F_y}\right|$$

The trafficability limit can be simply enhanced by increasing those traction forces. As mentioned in Fig. 5-(a), the drawbar pull has a maximum value at s=1.0, however a rover at s=1.0 is not able to travel anymore, and also, a wheel with high slip causes a soil destruction around the wheel. It is therefore needed to control each wheel to drive with an appropriate slip. Regarding the side force, the larger the slip angle is, the larger the side force becomes. If a steering angle of each wheel are properly given, a rover will traverse a slope. However in the case that a slope is covered with loose soil, the soil at the side face of the wheel performs like a snow avalanche when the wheel has a large enough side force to overcome the bearing stress of the soil. Hence, according to the above discussions, the trafficability limit is redefined as a limit of the soil bearing capacity.

5. Slope Traversability Experiments

The slope experiments using our rover test bed were conducted in order to analyze the traversability of a rover based on the criteria, the mobility limit and the trafficability limit. The experiments are divided into slope climbing and slope traversing experiments.

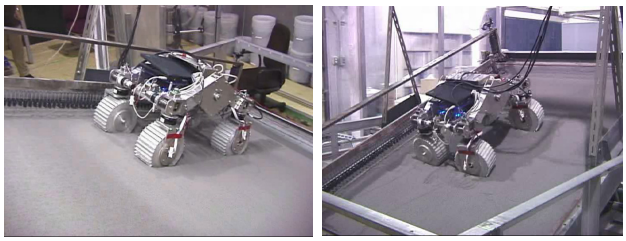

(a) : Slope climbing experiment (b) : Slope traversing experiment

Fig. 9: Slope traversability experiment

Table 2: Slope climbing experiment

Torque limit	Configuration	Max slope angle : (Criteria)
small	Config-A	14 [deg] : (Mobility limit)
small	Config-B	19 [deg] : (Mobility limit)
large	Config-A	21 [deg] : (Trafficability limit)
large	Config-B	21 [deg] : (Trafficability limit)

5.1 Experimental setup

Fig. 9 shows overviews of the experimental setup with our rover test bed. The facility, located at Japan Aerospace Exploration Agency (JAXA), in Chofu, JAPAN, consists of a flat rectangular vessel in the size of 1.5 by 2.0 [m] filled up with 10 [cm] depth of the Lunar Regolith Simulant. The vessel can be inclined up to 30 [deg].

The four-wheeled rover test bed developed by author's group has the dimension of 0.62 [m](length) × 0.53 [m](width) × 0.46 [m](height) and weighs about 35 [kg] in total. Each wheel of the rover is same as the wheel used in the single wheel experiment. All wheels have active steering DOF (Degree Of Freedom).

During the experiments, the rover test bed travels with a given angular velocity and a steering angle. Each wheel is controlled to travel with a constant angular velocity as 12 [rpm] and an arbitrary steering angle by an on-board computer. We measured a motion trajectory of the rover using 3D optical sensors. Force/torque sensors are mounted on upper part of each wheel to measure the forces generated by the corresponding wheel.

5.2 Slope climbing experiment and discussion

In the slope climbing experiment, the slope angle is given from 10 [deg] to the angle which the rover cannot climb up. The wheel driving motors are chosen two different types in a torque limit (small/large) to discuss the mobility limit. Also, the configurations of the rover are given two different centroid positions as the Config-A (center) and Config-B (front) as shown in Fig. 7.

The experimental results are summarized in Table 2. Through a number of the climbing experiment, the maximum slope angle for the slope climbing using the small torque motor is 14 [deg] because the motor was suspended. This result indicates that a resistance torque to the wheel might exceed the motor torque limit, and this was the mobility limit. On the other hand, the maximum slope angle using the large torque motor is 21 [deg] since the wheel has large slip (almost

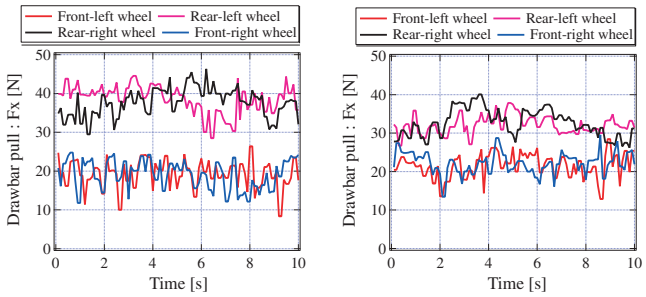

(a) : Config-A (b) : Config-B

Fig. 10: Time profile of drawbar pull

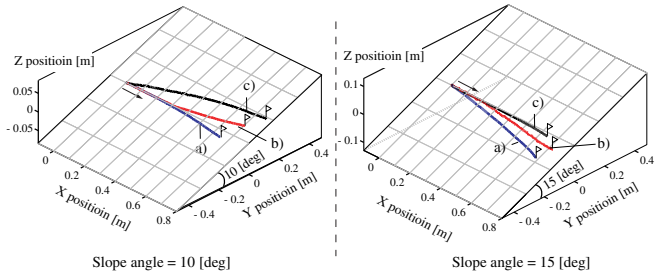

Fig. 11 : Slope traversing experiments (a):no steering, b):each of front wheels has 15 [deg], c):every wheel has 15 [deg].)

s=1.0) but does not suspended. The soil destructions around the driving wheel were observed in that slope angle. The trafficability limit gives this result as 21 [deg] for the maximum slope angle.

In the case of using the small torque motor, we found that the maximum slope angle with the Config-B was improved as 19 [deg], while the rover without shifting the centroid (Config-A) was able to climb up to only the slope of 14 [deg]. This result indicates that the resistance torque was successfully diminished by shifting the centroid of the rover ahead.

It must be emphasized that the effectiveness by shifting the centroid of the rover was not seen in the case of using the large torque motor. The reason is deduced that a summation of the drawbar pulls of all wheels is almost same value even in both cases. In fact, in the case of the slope angle of 21 [deg], the traction load of the rover L was 115 [N] and the summation of the drawbar pulls was about 110 $\sim$ 120 [N] in both rover configurations as shown in Fig. 10.

5.3 Slope traversing experiment and discussion

We also conducted the slope traversing experiment using the large torque motor. In this experiment at any arbitrary slope angles, the rover is given three different steering configurations; a) no steering, b) steer only front wheels with a steering angle of 15 [deg], and c) steer all wheels with a steering angle of 15 [deg].

According to the experimental result as shown in Fig. 11, it is clearly seen that the larger the slope angle becomes, the more significant a skid motion of the rover is, and then, the rover is not able to climb and traverse the slope angle of 15 [deg] with any steering configurations. The summation of the drawbar pulls and the side force must be smaller than the traction load of the rover. Thus, the slope angle of 15 [deg] is the trafficability limit in the cases of those steering configurations.

The skid motion on a slope generally subjects to the steering angles since a destructive phase at a side face of a wheel depends on a side force of the wheel. It is important issue to control the steering angle of each wheel to traverse a slope with considering the soil destruction.

6. Conlusion

This paper described the slope traversability analysis based on the terramechanics. The criteria dominating the slope traversability are elaborated and validated along with the single wheel experiments and the slope climbing/traversing experiments. The proposed criteria can be concluded that the mobility limit depends on a vehicle performance (e.g. motor torque and vehicle configuration), whereas the trafficability limit is determined by a wheel-and-soil interaction (soil destruction around a wheel.)

Based on the mobility limit, it is able to discuss what kind of motors is appropriate to a slope negotiation in a real mission. Moreover, using the trafficability limit, we can find a better control algorithm to climb/traverse a slope with avoiding a large slip/skid motion which may cause mission failure such as a rover stuck and tipover.

Acknowledgements

The authors would like to express their best thanks to Dr. Kohtaro Matsumoto and Dr. Sachiko Wakabayashi at Japan Aerospace Exploration Agency (JAXA), for providing opportunities of slope climbing/traversing experiments using their facility.

References

[1] M. G. Bekker; “Off-The-Road Locomotion,” The University of Michigan Press, 1960.
[2] M. G. Bekker; “Introduction to Terrain-Vehicle Systems,” The University of Michigan Press, 1969.
[3] J. Y. Wong; “Theory of Ground Vehicles,” John Wiley & Sons, 1978.
[4] K. Iagnemma, H. Shibly, S. Dubowsky; “On-Line Traction Parameter Estimation for Planetary Rovers,” Proc. of the 2002 IEEE Int. Conf. on Robotics and Automation, pp. 3142–3147, 2002.
[5] K. Iagnemma and S. Dubowsky,; “Mobile Robot in Rough Terrain,” Springer Tracts in Advanced Robotics, vol.12, 2004.
[6] K. Yoshida, N. Mizuno, G. Ishigami, A. Miwa, “Terramechanics-Based Analysis for Slope Climbing Capability of a Lunar/Planetary Rover,” 24th Int. Symp. on Space Technology and Science, 2004-k-06 2004.
[7] G. Ishigami and K. Yoshida ; “Steering Characteristics of an Exploration Rover on Loose Soil Based on All-Wheel Dynamics Model,” Proc of the 2005 IEEE Int. Conf. on Intelligent Robots and Systems, pp. 2041-2046, 2005.
[8] Wong, J. Y., Reece, A. R., “Prediction of Rigid Wheel Prefoemance Based on the Analysis of Soil-Wheel Stresses Part I, Preformance of Driven Rigid Wheels,” Journal of Terramechanics, vol.4, 1967.